RSC Advances

PAPER

View Article Online
View Journal | View Issue

Cite this: *RSC Adv.*, 2017, **7**, 40922

A first-principles study of anionic (S) and cationic (V/Nb) doped $Sr_2Ta_2O_7$ for visible light photocatalysis

Yuman Peng, †[ab] Zuju Ma, †[a] Junjie Hu[ab] and Kechen Wu*[a]

Received 27th June 2017
Accepted 14th August 2017

DOI: 10.1039/c7ra07113b

rsc.li/rsc-advances

In order to effectively utilize the visible solar light to catalyze and decompose water into hydrogen and oxygen, the ultraviolet light responsive photocatalyst $Sr_2Ta_2O_7$ is engineered *via* co-doping of the anionic (S) and cationic (V/Nb) to shift the VBM (valence band maximum) upward and CBM (conduction band minimum) downward by approximately 1 eV, respectively. By first principles study (GGA-PBE), it is discovered that the VBM of (S, V) co-doped $Sr_2Ta_2O_7$ is shifted upward by 1.14 eV while the CBM of this system is shifted downward by 0.68 eV, which is due to the appearance of impurity states near the VBM and CBM, respectively. For (S, Nb) co-doped $Sr_2Ta_2O_7$, the VBM is shifted upward by 0.74 eV and the CBM is shifted downward by 0.63 eV. No impurity states of Nd are created, neither near the CBM nor in the band gap for (S, Nb) co-doped case, probably because the $Sr_2Ta_2O_7$ is essentially isostructural with $Sr_2Nb_2O_7$. For these two systems mentioned above, it could be a feasible way for $Sr_2Ta_2O_7$ photocatalyst on water splitting under UV irradiation to convert into the visible light-utilizing material without introducing extra electrons or holes.

1. Introduction

Alternative sources of energy have been widely searched for over several decades due to the depletion of fossil fuel resources and increasingly serious environmental problems. It is quite possible for hydrogen to be the candidate. Today 95% of hydrogen in the world is produced *via* steam reforming of fossil fuels, which generates considerable greenhouse gases.[1] Hence, it is necessary to seek a feasible way for hydrogen production. A multitude of tantalates and niobates based layered perovskite structures, including $Sr_2Ta_2O_7$ and $Sr_2Nb_2O_7$,[2,3] have received intense attention as promising photocatalyst materials for water splitting and hydrogen production owing to their high photocatalytic activity, compared with the standard known bulk type of materials such as TiO_2.[4] It is reported that $Sr_2Ta_2O_7$ shows activities for water splitting into H_2 and O_2 in pure water even without additives under UV irradiation because of its high conduction level and the surface catalytic ability for H_2 evolution.[2] For strontium tantalates, the conduction band will become narrower and the band gap increases by the same amount when the bond angle O–M–O decreases from 180°. The bond angle O–Ta–O is close to 180° in $Sr_2Ta_2O_7$ which approaches to an ideal perovskite structure, thus implying that the excitation energy is more delocalized and the photo-generated electron–hole pairs in $Sr_2Ta_2O_7$ can more easily move.[2,5,6] Although $Sr_2Ta_2O_7$ is promising as the UV-light driven photocatalyst, it still fails to utilize effectively solar energy, especially for the region of visible light.

To achieve the maximum usage of sunlight, the semiconductor must have an optimal band gap. The suitable band gap for any visible light irradiated photocatalyst is around 2.0 eV. Furthermore, the valence band position should be more positive than the water oxidation potential (O_2/H_2O) and conduction band position should be more negative than hydrogen reduction potential (H^+/H_2).[7] Doping of foreign elements into UV-active photocatalyst[8–11] is a common strategy to design visible-light efficient photocatalyst. Mukherji *et al.* have designed a new type of composite containing graphene–Pt and $Sr_2Ta_2O_{7-x}N_x$ with an additional ~80% increase in hydrogen production and a quantum efficiency of 6.45% (~177% increase from pristine $Sr_2Ta_2O_7$).[12] Liu *et al.* discovered that the band gap of $Sr_2Ta_2O_7$ doped by the anionic (N)/cationic (Mo, W) is significantly reduced for visible light photocatalysis by the first-principles study.[13] According to the previous studies on $Sr_2Ta_2O_7$,[2,13] it is known that the valence band maximum (VBM) is 1.71 eV lower than the oxidation potential (H_2O/O_2) of water while the conduction valence minimum (CBM) is 1.66 eV higher than the reduction potential (H^+/H_2) in Fig. 1(a).

In this work, we intend to engineer the band gap by doping, where both the edge of the conduction band and valence band are differently shifted downward and upward by approximately 1 eV based on the primitive $Sr_2Ta_2O_7$. However, it might be

[a]State Key Laboratory of Structural Chemistry, Fujian Institute of Research on the Structure of Matter, Chinese Academy of Sciences, Fuzhou 350002, China. E-mail: wkc@fjirsm.ac.cn

[b]University of Chinese Academy of Sciences, Beijing 100049, P. R. China

† These authors have contributed equally.

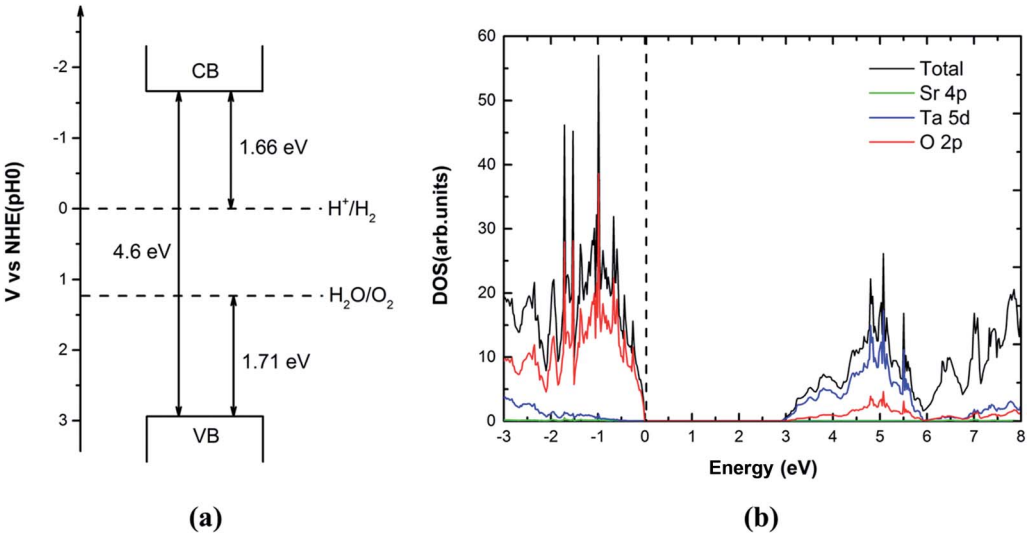

Fig. 1 (a) Band edge alignment of pure $Sr_2Ta_2O_7$ with respect to the water redox potentials. (b) The calculated total and partial density of states of primitive $Sr_2Ta_2O_7$ (using PBE). The vertical dashed line represents the Fermi level.

adverse for the stability of systems or create impurity states in the band gap if a single electron or hole is introduced in mono-doping.[14] In order to avoid the appearance of the unwanted states and keep stable for the doped $Sr_2Ta_2O_7$, the anionic element (sulfur) with a higher p orbital energy than that of the oxygen is chosen to dope at the O site while vanadium and niobium become the doped cationic elements to replace Ta. Afterwards, we have studied the (S–V/Nb) co-doped systems with different concentration of S or V/Nb and discussed the effects of mono- and co-doping on the electronic structure of $Sr_2Ta_2O_7$. We have calculated the formation energies for the mono and co-doped systems to predict the possibilities of such doping. The relative stabilities between the mono and co-doped $Sr_2Ta_2O_7$ systems are judged on their binding energies.

2. Computational details

The first-principles calculations have been performed using projected augmented wave (PAW) method,[15] as implemented in the Vienna ab initio simulation package (VASP).[16] For our calculations, the exchange correlation interaction is treated in the level of the GGA using Perdew–Burke–Ernzerhof (GGA-PBE).[17] The Brillouin zone was integrated using Monkhorst–Pack generated sets of *k*-points. The *k*-point meshes[18] of the Brillouin sampling for structural optimization and the density of states (DOS) calculations were set at $3 \times 1 \times 5$ and $5 \times 1 \times 5$, respectively. The plane cutoff energy of 550 eV was used to describe the electronic wave function. In all calculations, self-consistency was achieved with a tolerance in the total energy of at least 10^{-4} eV and with the residual force below 0.01 eV $Å^{-1}$. The PAW potentials with the valence states 4s, 4p and 5s for Sr, 2s and 2p for O, 6s and 5d for Ta, 3s and 3p for S, 3p, 3d and 4s for V, 4p, 5s and 4d for Nb have been used. For the doped cases, a $2 \times 1 \times 1$ supercell with 88 atoms (Sr : Ta : O = 16 : 16 : 56) was used, where the dopant anions or cations were substituting the O or Ta site of the supercell, respectively. In order to obtain the proper ground state structure, the spin polarized calculations are used for all the doped systems. The total and partial density of states of pure and the doped systems are aligned with respect to the O 2s core states, which is quite far from the doped atom.

3. Results and discussion

3.1. Primitive $Sr_2Ta_2O_7$

The TaO_6 octahedra interconnect in the original crystal of $Sr_2Ta_2O_7$ (its space group is *Cmcm*), thus forming layered

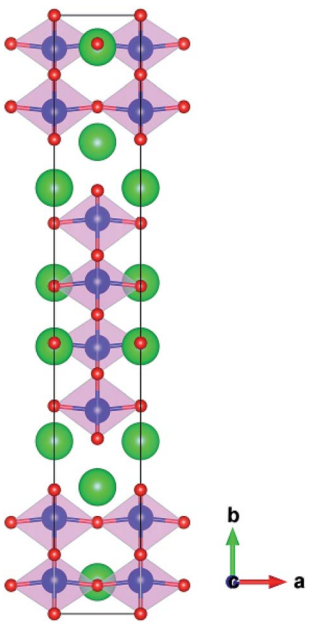

Fig. 2 The perovskite-slab structures of $Sr_2Ta_2O_7$ unit cell. The green, blue, red spheres represent Sr, Ta and O atoms, respectively; the pink regions represent TaO_6 octahedra.

Table 1 The lattice parameters and band gaps of calculation and experiment for $Sr_2Ta_2O_7$ unit cell

$Sr_2Ta_2O_7$ (*Cmcm*)	GGA-PBE	Experimental values
a (Å)	3.989	3.937
b (Å)	27.627	27.198
c (Å)	5.749	5.692
Band gap (eV)	2.88	4.60

perovskite structure (Fig. 2). The calculated lattice parameters of the unit cell and band gap by GGA-PBE are compared with the corresponding experimental values,[2,19] which are separately listed in the Table 1. The lattice parameters are predicted accurately whereas the band gap of primitive $Sr_2Ta_2O_7$ from GGA-PBE (2.88 eV) is much smaller than the experimental value (4.60 eV).[2] It is common that the GGA-PBE method tends to underestimate the band gap of metal oxides,[20] however, this method could correctly predict the shifts of the conduction band and valence band edge and energies of pure or doped structures. We have calculated the electronic structures, formation energies, relative binding energies and absorption spectra using GGA-PBE. Fig. 1(b) illustrates the total and partial densities of states about the primitive $Sr_2Ta_2O_7$. It is obvious that Ta 5d and O 2p orbitals dominate respectively in the bottom of conduction band and top of valence band,[13] which has been reported before. In the following sections, the cationic and anionic doping will be introduced to engineer the band gap.

3.2. S-Doping in $Sr_2Ta_2O_7$

In the S anionic mono-doping, we have replaced oxygen atoms in $Sr_2Ta_2O_7$ supercell with 88 atoms (Sr : Ta : O = 16 : 16 : 56) to tune the valence band edge and explore the effect of the neutral doping on band gap with the variable doping concentrations. Doping S atom is one of the potential methods to engineer the valence band edge, which has been reported in a large number of first-principles studies on metal oxides semiconductors.[11] This is because sulfur is isoelectronic to oxygen and it could avoid introducing the extra electrons or holes for the whole doped system after replacing O atom with S atom. Here we have demonstrated the band gaps of S-doped $Sr_2Ta_2O_7$ with various doping concentrations in Table 2. In addition, the shifts of the valence band maximum (VBM) and conduction band minimum (CBM) for all S-doped systems are also listed in this table. Their respective electronic structures by the spin polarized calculations will be presented in Fig. 3.

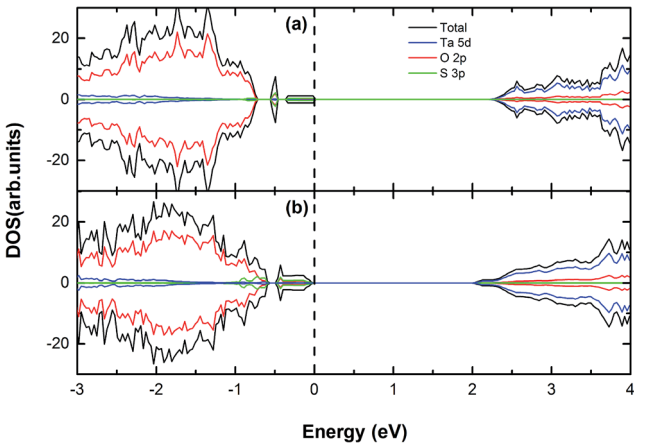

Fig. 3 The calculated (using PBE) DOS and PDOS for (a) S, (b) 2S doped $Sr_2Ta_2O_7$. The vertical dashed line represents the Fermi level.

From Table 2, there is the dependence of the band gap on S-doping concentration. The band gap reduces modestly to 2.24 eV with one sulfur atom doped, which can be attributed to the appearance of S impurity states merely above the valence band edge (Fig. 3(a)). Both VBM and CBM of this system move upward by 0.93 eV and 0.29 eV, respectively; as the S-doping concentration is increased, the corresponding band gap continues to decline to 2.03 eV ($C_{S\text{-doping}} = 3.57\%$) with the VBM shifted upward by 0.94 eV. According to Fig. 3(a) and (b), it reveals that the VBMs of S-doped $Sr_2Ta_2O_7$ mainly consist of O 2p and S 3p orbitals. Compared (a) with (b), the peaks of the occupied impurity states in (b) become more obvious and a proportion of impurity states even merge into the initial valence band edge. From the information above, S-doping in $Sr_2Ta_2O_7$ could engineer the location of valence band edge. The engineered VBM is still lower than the oxidation potential (H_2O/O_2) of water, which means it is still possible for converting water into oxygen. Moreover, this approach prevents the appearance of impurity states in the middle of the band gap, thus avoiding the forming of recombination centers.

3.3. V or Nb-doping in $Sr_2Ta_2O_7$

It has been found that the cationic doping can significantly lower down the CBM of the material.[21–23] V, Nb and Ta locate on the same row (subgroup V B) of the periodic table, which means it is possible to move the conduction band edge downward by the V or Nb substitution at the Ta site without introducing extra electrons or holes. In this section, we have completed the spin

Table 2 The band gaps (E_g) calculated by PBE according to the different S-doping concentration of $Sr_2Ta_2O_7$

Amount of S doped (amount of O atoms = 56)	$C_{S\text{-doping}}$ (doping concentrations)	E_g (eV)	VB shift (eV)	CB shift (eV)	ΔE_{form} (eV per f.u)
Primitive	Primitive	2.88	0	0	
1	1.78%	2.24	+0.93	+0.29	0.41
2	3.57%	2.03	+0.94	+0.09	0.72

Table 3 The band gaps (E_g) calculated by PBE according to the different V-doping concentration of $Sr_2Ta_2O_7$

Amount of V doped (amount of Ta atoms = 16)	$C_{V\text{-doping}}$ (doping concentrations)	E_g (eV)	VB shift (eV)	CB shift (eV)	ΔE_{form} (eV per f.u)
Primitive	0	2.88	0	0	
1	6.25%	1.82	+0.14	−0.92	0.34
2	12.5%	1.48	−0.10	−1.48	0.68

Table 4 The band gaps (E_g) calculated by PBE according to the different Nb-doping concentration of $Sr_2Ta_2O_7$

Amount of Nb doped (amount of Ta atoms = 16)	$C_{Nb\text{-doping}}$ (doping concentrations)	E_g (eV)	VB shift (eV)	CB shift (eV)	ΔE_{form} (eV per f.u)
Primitive	0	2.88	0	0	
4	25%	2.49	−0.22	−0.62	0.47
6	37.5%	2.42	−0.25	−0.71	0.70

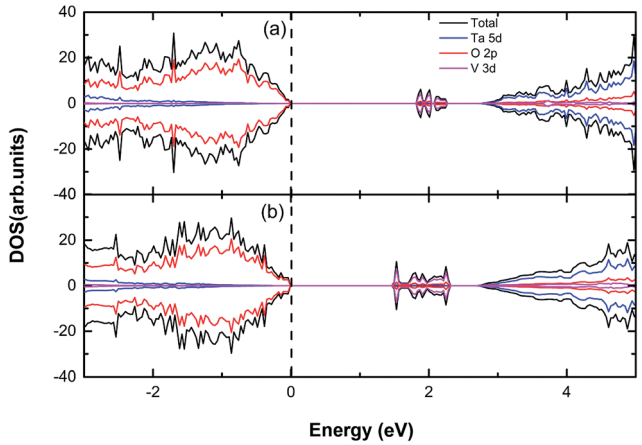

Fig. 4 The calculated (using PBE) DOS and PDOS for (a) V, (b) 2V doped $Sr_2Ta_2O_7$. The vertical dashed line represents the Fermi level.

polarized calculation of cationic V/Nb-doped systems and considered the relationship between the doping concentrations and the extent of CBM shifting, which is shown in Table 3 and 4.

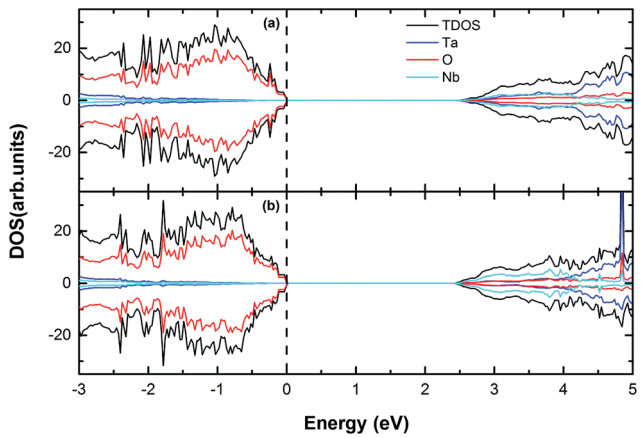

Fig. 5 The calculated (using PBE) DOS and PDOS for (a) 4Nb, (b) 6Nb doped $Sr_2Ta_2O_7$. The vertical dashed line represents the Fermi level.

The total and partial density of states (DOS) are plotted in Fig. 4 and 5, respectively.

When only one V atom is substituted for a Ta atom, the band gap dramatically declines to 1.82 eV and the CBM shifts downward by 0.92 eV, which might be suitable for tuning the conduction band edge on the purpose of hydrogen production. As the V doping concentration is increased to 12.5%, it is apparent that there is a significant decrease on the band gap (E_g = 1.48 eV) with the CBM moving downward by 1.48 eV. In Fig. 4(a) and (b), we can discover that several unoccupied impurity states appear in the band gap, which is due to the V-doping. The reason why there are impurity states in the band gap might be that V 3d orbital energy is considerably lower than that of Ta 5d.[24] Therefore, the effective band gap is reduced for V-doped $Sr_2Ta_2O_7$. However, the disadvantage of impurity states emerging in the band gap may be trapping the photo generated electrons and contributing to the electron–hole recombination. Furthermore, the range of impurity states will be extended if the V-doping concentration is increased, thus causing a drastic decrease of band gap. From the information mentioned, the band gaps, as well as the shifts of CBM, are affected dramatically by the V-doping concentration. The impurity states in the middle of band gap should be removed from the band gap so that the photochemical catalysis efficiency can be promoted.

Unlike V-doping, Nb-doping could slightly alter the CBM position in the band gap, where no impurity peak forms (Fig. 5). This may be because the radius of Nb atom is close to that of Ta atom and $Sr_2Ta_2O_7$ is essentially isostructural with $Sr_2Nb_2O_7$,[19] which means that the Nb 4d orbital energy is approximate to the Ta 5d orbital energy. The band gap is reduced to 2.49 eV with the CB shift of −0.62 eV and the VB shift of −0.22 eV when 4Nb doped. When six Nb atoms replace Ta atoms in $Sr_2Ta_2O_7$ supercell, the band gap is 2.42 eV with the CB shift of −0.71 eV and the VB shift of −0.25 eV (Table 4). However, it has been reported that the photocatalytic activity of $Sr_2Ta_2O_7$ was dramatically decreased by replacing tantalum with niobium because of lattice distortion around the niobium substituted

Table 5 The band gaps (E_g) of anionic (S) and cationic (V) co-doping in $Sr_2Ta_2O_7$ calculated by PBE according to the different S or V-doping concentrations

Amount of doped anionic atom(s)	Amount of doped cationic atom(s)	E_g (eV)	VB shift (eV)	CB shift (eV)	ΔE_{form} (eV per f.u)	E_b (eV)
1S	1V	1.47	+1.00	−0.40	0.72	0.21
1S	2V	1.30	+0.41	−1.17	1.08	0.02
2S	1V	1.43	+1.11	−0.35	1.17	−0.87
2S	2V	1.06	+1.14	−0.68	1.36	0.41
2S	6Nb	1.51	+0.74	−0.63	1.55	−0.51

and a lattice distortion may act as a recombination center for photo-induced electron–hole pairs.[25]

3.4. Anionic (S) and cationic (V/Nb) co-doping in $Sr_2Ta_2O_7$

To simultaneously move the VBM upward and the CBM downward by roughly 1 eV for decomposition of water under the visible light, we intend to tune the band gap by the anionic (S) and cationic (V/Nb) co-doping in $Sr_2Ta_2O_7$ with the S-doping or V/Nb-doping concentrations varied. These results of (S–V/Nb) co-doped groups have been recorded in Table 5. In addition, their electronic structures are shown in Fig. 6 and 7, respectively.

The effective band gap is declined with the VBM shifted upward by 1.00 eV and CBM shifted downward by 0.40 eV in (1S–1V) co-doped case. This is because S 3p and V 3d orbitals differently predominate the VBM and CBM, respectively (in Fig. 6(a)). Compared to the (1S, 1V) doped case, the shift-up of VBM becomes less obvious (only by 0.41 eV) with regard to the (S, 2V) co-doped system, whereas the CBM moves substantially downward (by 1.17 eV). Therefore, the shift-down of CBM could be ideal for the reduction reaction of water. In addition, the impurity states are in the vicinity of the conduction band edge instead of the middle of band gap (in Fig. 6(b)). For the (2S, V) and (2S, 2V) co-doped case, there are both considerable shift-ups of VBM (by 1.11 eV and 1.14 eV, respectively), which indicates that the engineering of VBM is accomplished. The CBM of the (2S, V) system only shifts downward by 0.35 eV, which is almost half of that of the (2S, 2V) co-doped system (by 0.68 eV). Therefore, the band gap of (2S, 2V) doped case (1.06 eV) is significantly narrower than that of (2S, V) doped $Sr_2Ta_2O_7$ (1.43 eV). In contrast to the DOS and PDOS of (c), there are

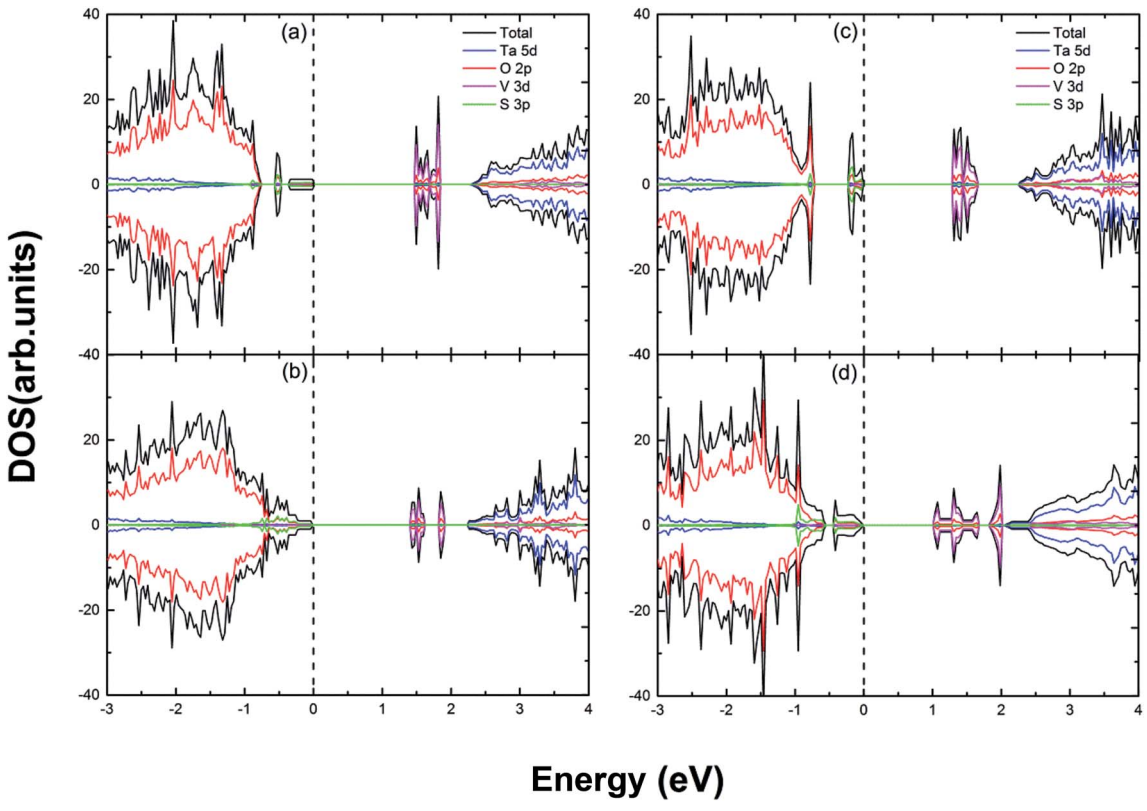

Fig. 6 The calculated (using PBE) DOS and PDOS for (a) S and V doped; (b) S and 2V doped; (c) 2S and V doped; (d) 2S and 2V doped $Sr_2Ta_2O_7$. The vertical dashed line represents the Fermi level.

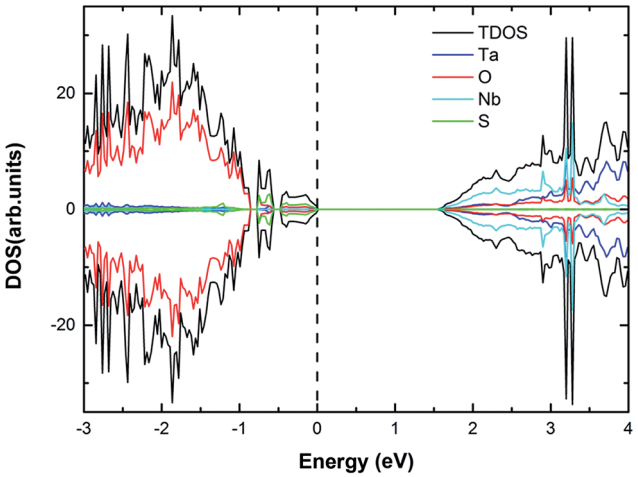

Fig. 7 The calculated (using PBE) DOS and PDOS for (2S, 6Nb) co-doped $Sr_2Ta_2O_7$. The vertical dashed line represents the Fermi level.

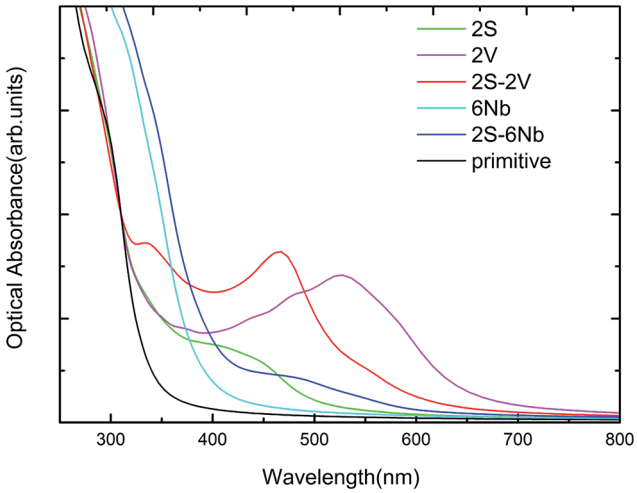

Fig. 8 The calculated optical absorption plots of anionic (S) or cationic (V/Nb) mono-doping with different concentrations and co-doping of S and V/Nb in comparison with pure $Sr_2Ta_2O_7$.

impurity states in close proximity to conduction band, thus creating a clean band gap in Fig. 6(d).

For (2S, 6Nb) co-doped $Sr_2Ta_2O_7$, the VBM is moved upward by 0.74 eV and the CBM is shifted downward by 0.63 eV. According to the DOS and PDOS (Fig. 7), the impurity states of sulfur atoms are generated above the valence band edge while no impurity states of Nb appear near the CBM. The position of VBM, coincident with CBM, is tuned reasonably by (2S–2V) and (2S–6Nb) co-doping in $Sr_2Ta_2O_7$ not only to prevent the recombination centers appearing but also to broaden the range of solar light absorption.

3.5. The formation energy and the relative binding energy of doped $Sr_2Ta_2O_7$

The formation energy (ΔE_{form}) for such doping concentration is being calculated using the following equation:[26]

$$\Delta E_{form} = E_T(D) - E_T(H) + n\mu_X - n\mu_Y$$

here $E_T(D)$ and $E_T(H)$ are the total energies of doped and pure $Sr_2Ta_2O_7$, respectively, and n is the number of the doping atoms. μ_X and μ_Y are the atomic potential of the host and dopant atoms, respectively. The calculated (using GGA-PBE) formation energies for the doped $Sr_2Ta_2O_7$ are listed in the tables ahead. In summary, the cationic V mono-doping is more favorable than others.

The relative stability between the co-doped and mono-doped systems is judged on the relative binding energy, the calculation formula of which is as follow:[26]

$$\Delta E_b = E(A) + E(B) - E(A + B) - E(pure)$$

In this equation, $E(A)$, $E(B)$ and $E(A + B)$ are total energies of the anion mono-doped, cationic mono-doped and co-doped systems, respectively. $E(pure)$ represents the total energy of the primitive $Sr_2Ta_2O_7$. The relative binding energies of the (S, V), (S, 2V), (2S, V), (2S, 2V) and (2S, 6Nb) co-doped systems are 0.21, 0.02, −0.87, 0.41 and −0.50 eV (Table 5), respectively. The positive value indicates that co-doping is more favorable in comparison to the mono-doping in $Sr_2Ta_2O_7$. Hence, the (2S, 2V) co-doped system is likely to be more stable than the others.

3.6. Absorption curves

We have studied the optical absorption spectra for the anionic (S) or cationic (V/Nb) mono-doping and co-doping of S and V/Nb with different concentrations using the PBE method, which is compared with the primitive $Sr_2Ta_2O_7$ and presented in Fig. 8. It shows that 2V mono-doping, (2S–2V) co-doping could harvest longer wavelength of visible light spectrum as compared to the primitive $Sr_2Ta_2O_7$ for efficient photocatalyst. The absorption peaks of these 2S-doped, 2V-doped, 6Nb-doped, (2S–2V) and (2S–6Nb) co-doped $Sr_2Ta_2O_7$ are mainly attributed to the electrons transition from S 3p orbitals to the CBM, from the VBM to V 3d orbitals, from the VBM to Nb 4d orbitals, from S 3p to V 3d orbitals and from S 3p to Nb 4d orbitals, respectively.

4. Conclusion

The electronic structures of S and V/Nb mono- and (anionic–cationic) co-doped $Sr_2Ta_2O_7$ have been studied on the band gap engineering and the shifts of the VBM and CBM for sufficiently utilizing visible light of the solar spectrum by GGA-PBE calculations. It is successful for the anionic (S) doped $Sr_2Ta_2O_7$ to tune the location of the valence band edge with the S-doping concentration varied, thus moderately shifting the VBM upward by approximately 1 eV. Owing to no single electron or hole created, the occupied or unoccupied states of dopants are prevented in the band gap from becoming recombination centers. In the case of the (V) cationic doped systems, the significant shift-down of CBM is a result of the appearance of impurity states mixing between O 2p and V 3d. As the V-doping concentration increases, the extent of the CBM shift-down

becomes more obvious (by 0.92 and 1.48 eV, respectively). Unlike the V-doped systems, Nb doping in $Sr_2Ta_2O_7$ could shift mildly the CBM downward (only by 0.6–0.7 eV) without any impurity states appearing near the CBM. To simultaneously achieve the tuning of VBM and CBM, we have performed the S and V/Nb co-doped cases, from which the VBM is moved upward by 1.14 and 0.74 eV and the CBM is moved downward by 0.68 and 0.63 eV for (2S–2V) and (2S, 6Nb) co-doped $Sr_2Ta_2O_7$, respectively. Both systems still remain "clean" for the band gap and capable of catalyzing water into hydrogen and oxygen.

Conflicts of interest

There are no conflicts to declare.

Acknowledgements

This work was supported by the National Science Foundation of China (No. 21673240 and 21501177), the NSF of Fujian Province (No. 2017J05033) and the Foreign Cooperation Project of Fujian Province (No. 2017I0019). The authors gratefully acknowledge the Supercomputing Center of CNIC for providing the computing resources.

References

1 B. C. Wang, *et al.*, Band gap engineering in $BiNbO_4$ for visible-light photocatalysis, *Appl. Phys. Lett.*, 2012, **100**(18), 182102.
2 A. Kudo, H. Kato and S. Nakagawa, Water splitting into H-2 and O-2 on new $Sr_2M_2O_7$ (M = Nb and Ta) photocatalysts with layered perovskite structures: factors affecting the photocatalytic activity, *J. Phys. Chem. B*, 2000, **104**(3), 571–575.
3 Y.-M. Song, J.-Q. Dai and H. Zhang, Hybrid functional study on optical properties of $Sr_2M_2O_{7-x}N_x$ (M = Nb, Ta) photocatalysts with perovskite-slab structures, *Curr. Appl. Phys.*, 2016, **16**(1), 1–7.
4 X. B. Chen, *et al.*, Semiconductor-based photocatalytic hydrogen generation, *Chem. Rev.*, 2010, **110**(11), 6503–6570.
5 H. Kato and A. Kudo, Water splitting into H-2 and O-2 on alkali tantalate photocatalysts ATaO(3) (A = Li, Na, and K), *J. Phys. Chem. B*, 2001, **105**(19), 4285–4292.
6 K. Yoshioka, *et al.*, The relationship between photocatalytic activity and crystal structure in strontium tantalates, *J. Catal.*, 2005, **232**(1), 102–107.
7 A. Kudo and Y. Miseki, Heterogeneous photocatalyst materials for water splitting, *Chem. Soc. Rev.*, 2009, **38**(1), 253–278.
8 P. Kanhere, *et al.*, Mono- and co-doped $NaTaO_3$ for visible light photocatalysis, *Phys. Chem. Chem. Phys.*, 2014, **16**(30), 16085–16094.
9 P. Liu, *et al.*, Anion–anion mediated coupling in layered perovskite $La_2Ti_2O_7$ for visible light photocatalysis, *J. Phys. Chem. C*, 2013, **117**(27), 13845–13852.
10 Z. Ma, *et al.*, Mechanism of enhanced photocatalytic activities on N-doped $La_2Ti_2O_7$: an insight from density-functional calculations, *Int. J. Hydrogen Energy*, 2015, **40**(2), 980–989.
11 J. Nisar, *et al.*, Hole mediated coupling in $Sr_2Nb_2O_7$ for visible light photocatalysis, *Phys. Chem. Chem. Phys.*, 2012, **14**(14), 4891–4897.
12 A. Mukherji, *et al.*, Nitrogen doped $Sr_2Ta_2O_7$ coupled with graphene sheets as photocatalysts for increased photocatalytic hydrogen production, *ACS Nano*, 2011, **5**(5), 3483–3492.
13 P. Liu, *et al.*, Layered perovskite $Sr_2Ta_2O_7$ for visible light photocatalysis: a first principles study, *J. Phys. Chem. C*, 2013, **117**(10), 5043–5050.
14 J. Nisar, *et al.*, Mo- and N-doped $BiNbO_4$ for photocatalysis applications, *Appl. Phys. Lett.*, 2011, **99**(5), 3.
15 P. E. Blochl, Projector augmented-wave method, *Phys. Rev. B*, 1994, **50**(24), 17953–17979.
16 G. Kresse and D. Joubert, From ultrasoft pseudopotentials to the projector augmented-wave method, *Phys. Rev. B*, 1999, **59**(3), 1758–1775.
17 J. P. Perdew, K. Burke and M. Ernzerhof, Generalized gradient approximation made simple, *Phys. Rev. Lett.*, 1996, **77**(18), 3865–3868.
18 J. D. Pack and H. J. Monkhorst, Special points for Brillouin-zone integrations, *Phys. Rev. B*, 1976, **13**(12), 5188–5192.
19 N. Ishizawa, *et al.*, Compounds with perovskite-type slabs.2. crystal-structure of $Sr_2Ta_2O_7$, *Acta Crystallogr., Sect. B: Struct. Sci.*, 1976, **32**, 2564–2566.
20 R. W. Godby, M. Schluter and L. J. Sham, Accurate exchange–correlation potential for silicon and its discontinuity on addition of an electron, *Phys. Rev. Lett.*, 1986, **56**(22), 2415–2418.
21 W.-J. Yin, *et al.*, Band structure engineering of semiconductors for enhanced photoelectrochemical water splitting: the case of TiO_2, *Phys. Rev. B*, 2010, **82**(4), 045106.
22 A. Bokare, M. Pai and A. A. Athawale, Surface modified Nd doped TiO_2 nanoparticles as photocatalysts in UV and solar light irradiation, *Sol. Energy*, 2013, **91**, 111–119.
23 E. Garskaite, *et al.*, The study of preparation and photoelectrical properties of chemical bath deposited Zn, Sb and Ni-doped $CuInS_2$ films for hydrogen production, *Sol. Energy*, 2012, **86**(9), 2584–2591.
24 S.-H. Wei, H. Krakauer and M. Weinert, Linearized augmented-plane-wave calculation of the electronic structure and total energy of tungsten, *Phys. Rev. B*, 1985, **32**(12), 7792–7797.
25 M. Yoshino and M. Kakihana, Polymerizable complex synthesis of pure $Sr_2Nb_xTa_{2-x}O_7$ solid solutions with high photocatalytic activities for water decomposition into H-2 and O-2, *Chem. Mater.*, 2002, **14**(8), 3369–3376.
26 W. J. Yin, *et al.*, Double-hole-mediated coupling of dopants and its impact on band gap engineering in TiO_2, *Phys. Rev. Lett.*, 2011, **106**(6), 066801.

